JACS
JOURNAL OF THE AMERICAN CHEMICAL SOCIETY

Article

pubs.acs.org/JACS

Enhanced Emission from Single Isolated Gold Quantum Dots Investigated Using Two-Photon-Excited Fluorescence Near-Field Scanning Optical Microscopy

Neranga Abeyasinghe,[†] Santosh Kumar,[‡] Kai Sun,[§] John F. Mansfield,[§] Rongchao Jin,[‡] and Theodore Goodson III*[,†]

[†]Departmentof Chemistry, University of Michigan, Ann Arbor, Michigan 48109, United States

[‡]Departmentof Chemistry, Carnegie Mellon University, Pittsburgh, Pennsylvania 15213, United States

[§]Departmentof Materials Science and Engineering, Universityof Michigan, Ann Arbor, Michigan 48109, United States

Supporting Information

ABSTRACT: New approaches in molecular nanoscopy are greatly desired for interrogation of biological, organic, and inorganic objects with sizes below the diffraction limit. Our current work investigates emergent monolayer-protected gold quantum dots (nanoclusters, NCs) composed of 25 Au atoms by utilizing two-photon-excited fluorescence (TPEF) near-field scanning optical microscopy (NSOM) at single NC concentrations. Here, we demonstrate an approach to synthesize and isolate single NCs on solid glass substrates. Subsequent investigation of the NCs using TPEF NSOM reveals that, even when they are separated by distances of several tens of nanometers, we can excite and interrogate single NCs individually. Interestingly, we observe an enhanced two-photon absorption (TPA) cross section for single Au_{25} NCs that can be attributed to few-atom local field effects and to local field-induced microscopic cascading, indicating their potential for use in ultrasensitive sensing, disease diagnostics, cancer cell therapy, and molecular computers. Finally, we report room-temperature aperture-based TPEF NSOM imaging of these NCs for the first time at 30 nm point resolution, which is a ~5-fold improvement compared to the previous best result for the same technique. This report unveils the unique combination of an unusually large TPA cross section and the high photostability of Au NCs to (non-destructively) investigate stable isolated single NCs using TPEF NSOM. This is the first reported optical study of monolayer-protected single quantum clusters, opening some very promising opportunities in spectroscopy of nanosized objects, bioimaging, ultrasensitive sensing, molecular computers, and high-density data storage.

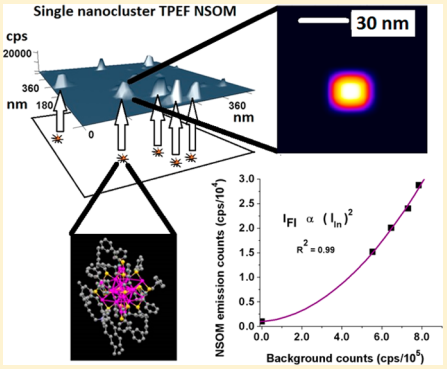

1. INTRODUCTION

Quantum-confined monolayer-protected noble metal nanoclusters (NCs, with metal core diameters <2.5 nm) have recently emerged as a novel class of nanomaterials following the first determination of their crystal/atomic structure[1−7] and the demonstration of their remarkable catalytic,[8] electronic,[9] magnetic,[10] and optical properties.[11−15] These unique properties in NCs are due to the band gap opening as their metal core diameters approach the Fermi wavelength of free valence electrons, an effect termed *quantum confinement*. Even though their optical properties were studied extensively for NC ensembles,[11−15] no evidence of *single NC optical properties* has been reported until the current work. The advantage of single NC (single molecule) investigations is that they manage to draw out many intricate and fundamental details of individual nanoclusters/molecules and effects of heterogeneity that are lost due to ensemble averaging; the NCs' unique individual behaviors can serve as reporters of their immediate nanoenvironments.[16] Therefore, probing of single NCs is desired to further appreciate the unique optical, electronic, and catalytic properties of these nanomaterials. Previously reported single NC investigations were conducted using electron microscopic techniques [e.g., high-angle annular dark-field (HAADF) scanning transmission electron microscopy (STEM) imaging or, combined with electron energy loss spectroscopy (EELS), aberration-corrected (AC) transmission electron microscopy (TEM)] that tend to perturb and alter the structure of the NC while it is being investigated.[2,7,17,18] If one is to use the NCs in bioimaging and sensing applications, electron microscopy becomes incompatible due to the high likelihood of damaging or altering the metal core structure.[7] For this reason, so far, room-temperature TEM investigations of isolated monolayer-protected clusters have not been reported for stable clusters smaller than Au_{55}.[19] Additionally, since single NCs can be utilized in many potential applications (e.g., sensing, bioimaging, and electronics), it is desired to study them using an approach that can likely be utilized in such

Received: July 26, 2016
Published: November 29, 2016

DOI: 10.1021/jacs.6b07737
J. Am. Chem. Soc. 2016, 138, 16299−16307

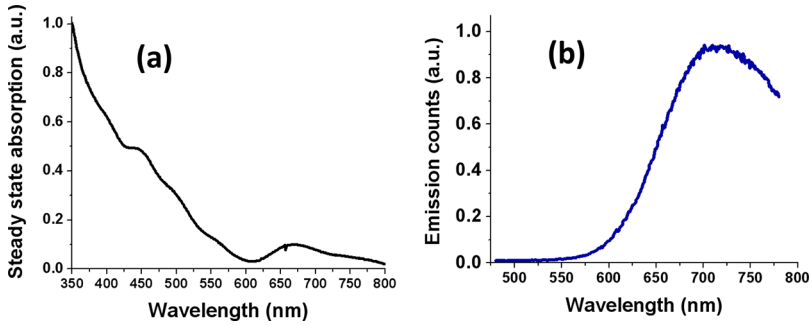

Figure 1. Steady-state absorption and emission spectra of $Au_{25}SG_{18}$ nanoclusters (NCs) in solution. (a) Steady-state absorption spectrum of the solution-phase quantum-confined Au_{25} SG_{18} NCs dissolved in water. The typical characteristic peaks for Au_{25} NCs are observed with an optical bandgap of about ∼1.80 eV. (b) Steady-state emission spectrum for the same solution when excited at 400 nm. As can be observed, the maximum emission appears at ∼700 nm.

endeavors. Therefore, in order to learn potentially promising properties of single nanoclusters, optical spectroscopy and microscopy are ideal owing to the non-destructive nature of optical excitation. More importantly, since quantum-confined NCs can have exceptional optical properties due to their unique electronic structures,[11−15] one may be able to exploit such properties to conduct single NC spectroscopy. Thus, with the aim of interrogating and eliciting the unique properties of single NCs in a non-invasive and non-destructive manner, novel approaches for studying the unique optical properties of quantum-confined NCs are desired.

Many advances in optical imaging and spectroscopy of nanoscale objects have been reported during the past few decades.[20−31] The ability to obtain point resolutions below the diffraction limit (∼λ/2; >200 nm for optical microscopy) was considered major progress, as it allowed closely spaced nanosized objects to be probed when they are tens of nanometers apart. Point resolution of a microscope can be defined as the full width at half-maximum (fwhm) of the representative point spread function (PSF) obtained from a single-point-like object. For far-field optical microscopy, improvement of point resolution below 200 nm required modification of the excitation or detection mechanism.[20−23] It was generally considered that, if a molecule has a nonlinear optical response, diffraction-unlimited point resolution can be attained readily.[21] Nonetheless, with far-field two-photon-excited fluorescence (TPEF) imaging, the excitation spot in the $x-y$ plane (lateral) will be twice as large as its one-photon counterpart.[21] Consequently, typical far-field multi-photon fluorescence microscopy[32] has not been able to enhance the lateral point resolution below 200 nm. (It must be noted that, in recent reports on nonlinear microscopy of metals, researchers were able to obtain *localization accuracy* at nanometer dimensions. Localization accuracy derives from a numerical determination of the precision of the maximum of PSF.[33,34]) Due to the use of longer wavelengths for excitation, multi-photon fluorescence microscopy has the advantage of lower background fluorescence, and due to the quadratic dependence of fluorescence on excitation intensity, improved contrast of the optical image is observed.[30]

Contrary to far-field techniques, near-field optical imaging eliminates the diffraction barrier altogether by using evanescent fields near ($\ll\lambda$) a sharp metal tip or an aperture (by reducing the effective excitation volume).[24−30] Betzig et al.[24] demonstrated room-temperature one-photon-excited fluorescence (1PEF) near-field scanning optical microscopy (NSOM) with point resolutions below 100 nm. Compared to 1PEF NSOM, multi-photon-excited fluorescence (e.g., TPEF) NSOM is also able to realize an enhanced point resolution due to its independence of diffraction by lateral confinement of light and strong intensity dependence inherent to two-photon excitation. In other words, TPEF NSOM carries all of the advantages of typical TPEF microscopy *and* the ability to (unlike far-field TPEF) obtain sub-diffraction point resolutions. Along these lines, TPEF NSOM of Rhodamine B single molecules was reported by Steel and co-workers.[35] However, point resolutions better than ∼175 nm were not found for aperture-based TPEF NSOM. It was inferred that, with smaller diameters of the apertures, insufficient intensities of the electric field component at the optical near field may have caused this difficulty.[35] Also, rapid photodamage of typical organic TPEF chromophores under high TPEF excitation intensities clearly limits the success of this approach. However, since noble metal NCs have demonstrated high stability under optical excitation, we explored the possibility of employing (while revealing) exceptional TPEF properties of NCs[15] for the interrogation of single isolated NCs with the TPEF NSOM technique that will also afford lateral resolutions an order of magnitude below the diffraction barrier. This could allow us to place the individual NCs on a substrate several tens of nanometers apart and investigate their nonlinear optical properties by exciting one NC at a time.

Previous investigations on 25-atom gold nanoclusters (Au_{25} NCs) revealed exceptionally large two-photon absorption (TPA) cross sections in the solution-phase NCs (δ = 4.27 × 10^5 GM [GM = 10^{-50} cm^4·s/photon])[15] and in NC films ($\delta \approx 10^6$ GM),[36] highlighting their potential to be used in multi-photon single NC spectroscopy. Also, Au NCs have shown enhanced emission quantum yields in the solution phase ($\eta \geq 1 \times 10^{-4}$),[37] orders of magnitude higher than those of their larger (>2.5 nm core diameter) counterparts such as gold nanoparticles (Au NPs) ($\eta \approx 10^{-6}$)[38,39] and smooth gold films[40] ($\eta \approx 10^{-10}$). Since water-soluble $Au_{25}SG_{18}$ (glutathione-protected Au_{25}) can be easily synthesized with high monodispersity,[41−43] it can potentially be used in biological imaging applications. Moreover, compared to Ag NCs, Au NCs are well studied and possess greater chemical stability,[44] and Cu NCs were not reported to possess unusually high TPA cross sections. Out of all of the Au NCs that have been studied so far, Au_{25} NCs are the most stable. Nonetheless, as mentioned earlier, no monolayer-protected single NC study (room-temperature TEM or optical) has been reported for *stable* monolayer-

DOI: 10.1021/jacs.6b07737
J. Am. Chem. Soc. 2016, 138, 16299−16307

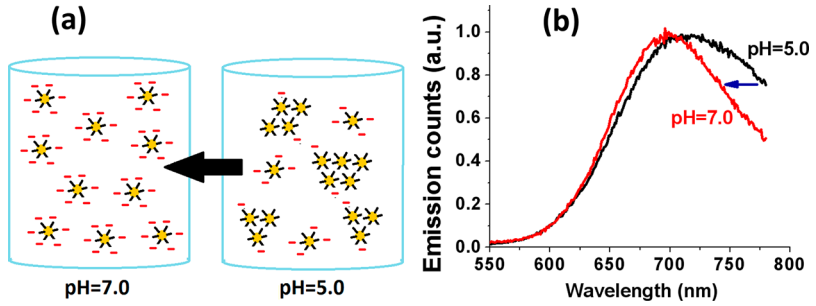

Figure 2. Isolation of $Au_{25}SG_{18}$ single nanoclusters in solution and corresponding steady-state emission spectra at elevated pH values. (a) Schematic of pH control: When moving from pH = 5.0 to pH = 7.0 solutions, $Au_{25}SG_{18}$ NCs get a completely negatively charged spherical environment, causing strong inter-nanocluster repulsion, which should render the isolation of single NCs in solution. Orange color corresponds to Au_{25} NC metal atom cluster, black to glutathione ligands, and red to representative negative charges due to ionization of carboxylic end groups of the glutathione (monolayer) ligands. (b) The steady-state emission of $Au_{25}SG_{18}$ gets narrower (shown by blue arrow) when moving from pH = 5.0 to pH = 7.0 solutions, consistent with the single NC isolation in the solution phase.

protected NCs smaller than Au_{55}.[19] Therefore, given the extraordinarily high stability reported for Au_{25} NCs,[44] their relatively smaller size (~1.2 nm), and their low biotoxicity compared to semiconductor quantum dots,[45] Au_{25} NCs are strong candidates for being adopted in high-resolution optical imaging, high-density data storage, and ultrasensitive sensing of nanoenvironments.

In this Article, using the aperture-based TPEF NSOM imaging technique, we report the first observations of single $Au_{25}SG_{18}$ NCs by demonstrating exceptional TPEF properties of the material. We investigate their dissolution into *single* NCs in solution and confirm the presence of isolated single NCs on solid substrates by utilizing STEM/TEM. We probe their optical properties at ~30 nm ($\sim\lambda/27$) point resolution using aperture-based TPEF NSOM while exciting one NC at a time. Therefore, in the current work, we report the utilization of the unusual nonlinear optical properties of NCs for their interrogation at single NC concentrations, which is a unique and non-destructive approach to obtain, confirm, and conduct single NC nonlinear spectroscopy and imaging.

2. RESULTS AND DISCUSSION

2.1. Steady-State Spectroscopy. $Au_{25}SG_{18}$ dissolved in water produces a steady-state UV−visible absorption spectrum (Figure 1a) with the characteristic absorption features observed for 400 nm (3.10 eV), 450 nm (2.76 eV), and 690 nm (1.80 eV). These absorption features indicate the strongly monodisperse nature and the characteristics of quantum confinement in Au_{25} NCs. If the NC sample contained many different sizes of NCs, they would cause a smoothening and disappearance of the specific absorption features observed due to slightly different absorption energies for different sizes. The synthetic procedure has been optimized previously to obtain monodisperse NCs with atomic precision (through size focusing;[41−43] see Experimental Section for more details). Also, when excited at 400 nm, water-soluble $Au_{25}SG_{18}$ NCs show an emission feature at ~700 nm (Figure 1b). This is consistent with the previous steady-state emission observed for $Au_{25}SG_{18}$ NC solutions and can be attributed to the lowest lying transition that was observed within the visible wavelengths.

2.2. Preparing Isolated Single Nanoclusters on Substrate. Even though one can assume that $Au_{25}SG_{18}$ NCs are not aggregated due to dissolution in water, there is no confirmation as to whether they are actually isolated from one another. This issue becomes critical when it comes to single NC spectroscopy and microscopy, as aggregate responses could be different from those of the isolated NCs. Therefore, pH = 7.2 solutions and a total of 2 min sonication time (in two 1-min sonication steps) were used for dissolving $Au_{25}SG_{18}$ NCs. Since 18 glutathione ligands each have two ionizable carboxylic groups (pK_1 = 2.12, pK_2 = 3.53), at pH = 7.2, we hypothesized that the NCs will form complete negatively charged ions on the distant carboxylic ends of the ligands, causing Coulombic repulsion between single NCs to occur (Figure 2a).[46] This approach should not only facilitate the complete dissolution of $Au_{25}SG_{18}$ NCs in water, but it also should ensure that the isolated single NCs are prevented from aggregation while they are in solution.

Interestingly, as depicted in Figure 2b, when the pH of the solution was changed from pH = 5.0 to pH = 7.0, the steady-state emission spectrum narrowed significantly (by approximately 100 nm). In contrast, the steady-state absorption spectra for the two solutions with different pH values appear almost the same, with about <10 nm blue shift for the pH = 7.0 $Au_{25}SG_{18}$ NC solution (see Figure S6). This clearly agrees with our aforementioned hypothesis that the Au_{25} NC aggregation occurring at pH = 5.0 causes an increase in the emissive densities of states that results in a broader emission spectrum compared to that of pH = 7.0 solution. Since the NC steady-state absorption is largely affected by its 13-gold-atom icosahedral core structure,[3] the effect of aggregation in pH = 5.0 solution on absorption appears to be minimal, since most of the effects of aggregation or close proximity are likely felt only by the surface emissive states (except through symmetry).

2.3. Confirming Isolated Single Nanoclusters Using Scanning Transmission Electron Microscopy/Transmission Electron Microscopy. In order to confirm that the TPEF NSOM samples would contain isolated single NCs on the substrate, we have conducted STEM/TEM imaging experiment for Au_{25} NC solutions (pH = 7.2) drop-cast on holey-carbon copper grids and air-dried for >10 min. These solutions were ~85-fold more concentrated than the solutions used for spin-coating of the samples prepared for the TPEF NSOM experiment, which will be discussed later (Figure 5). As can be seen in Figure 3a,b, we were able to observe isolated single $Au_{25}SG_{18}$ NCs on the substrate, even with very slow evaporation of the solvent and at 120 nM concentration. From the size histogram analysis (Figure S2), >80% of the STEM image features show a diameter of 1.21 ± 0.15 nm, confirming single isolated Au_{25} NCs, while ~17% of the features had

DOI: 10.1021/jacs.6b07737
J. Am. Chem. Soc. 2016, 138, 16299−16307

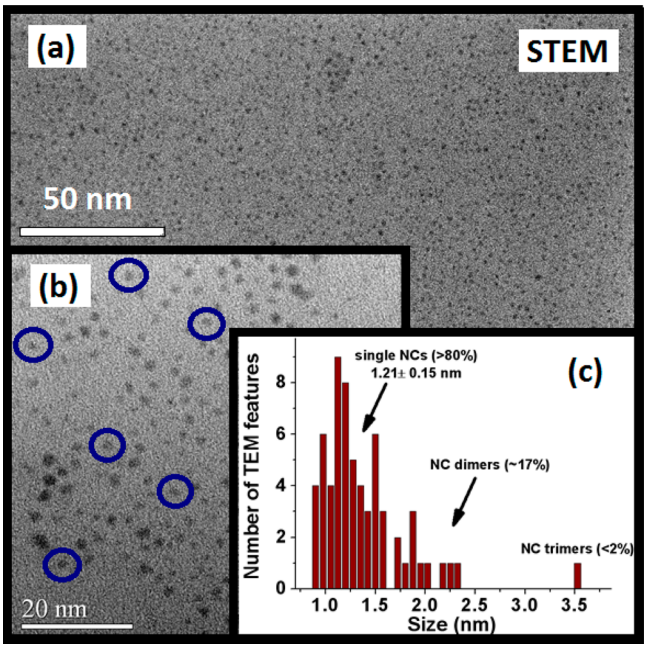

Figure 3. Au_{25} single-nanocluster STEM bright-field (BF) images; drop-cast film for ~85-fold higher concentration. (a) STEM (BF) image of Au_{25} SG_{18} NCs drop-cast on holey-carbon copper grid for 120 nM $Au_{25}SG_{18}$ solution dissolved in pH = 7.2 solution. STEM (BF) field of view is 225 nm × 225 nm. Slow drying of the sample took >10 min. (b) STEM image of the same area with higher resolution. A few single NC images are circled in blue. (c) From the STEM (BF) image size distribution analysis, we observed >80% of single Au_{25} NCs with 1.21 ± 0.15 nm mean diameter; ~17% of the TEM features observed were from Au_{25} NC dimers, and <2% of the features correspond to Au_{25} NC trimers. Au_{25} SG_{18} NC density ~16,300 NCs/μm^2. Since the solutions used for TPEF NSOM sample preparation had ~85 times lower NC concentrations, the likelihood of dimer formation can be estimated to be <0.1%. Therefore, it is clear that our samples used for TPEF NSOM investigations contained isolated single Au_{25} NC densities on plasma-cleaned glass substrate (see Supporting Information for details).

diameters and shapes consistent with the sizes and shapes of Au_{25} NC dimers. Only <2% of the NCs formed Au_{25} NC trimers. This further proves that the technique using pH = 7.2 indeed had rendered strong inter-nanocluster repulsion. For the TPEF NSOM scans discussed later (Figure 5a), we used 1.4 nM solutions of Au_{25} NCs (pH = 7.2), which are 85-fold diluted compared to the solutions used for STEM. Therefore, the inter-nanocluster collision frequency of 1.4 nM solutions should be reduced by 85 times. This implies that, for the 1.4 nM concentrations used for spin-coating of single NCs on solid substrates (Figure 5a), we should expect <0.1% likelihood for any form of Au_{25} NC aggregation (see Supporting Information for more details). Also, from our observation of average inter-nanocluster distances of ~7.8 nm for 120 nM solutions drop-cast on solid substrate, we estimated the average inter-nanocluster distances for 1.4 nM solution spin-coated on glass substrate to be around 160 nm. This implies that the surface density of nanoclusters is 39 NCs/μm^2, which agrees well with the ~23 NCs/μm^2 observed for TPEF NSOM (see Figure 5 and the Supporting Information).

The spectroscopic evidence reported in sections 2.1 and 2.2 and the STEM characterization indicated above clearly indicate that single $Au_{25}SG_{18}$ NCs can be isolated in solution through pH control. Using these pH = 7.2 solutions, we have prepared 1.4 nM solutions of $Au_{25}SG_{18}$ NCs, and 4 μL volumes of them were spin-coated using 1400 rpm speeds on plasma-cleaned glass coverslips (see Experimental Section for details). The samples were then oven-dried under vacuum and subsequently used to conduct TPEF NSOM experiments.

Also, as indicated in Figure S7, we carried out concentration-dependent atomic force microscopy (AFM) studies on Au_{25} NCs in the absence of pH increase to pH = 7.0, which gave clear evidence of aggregation as the concentration was increased. The feature diameters tend to increase slightly, while the feature density (i.e., number of AFM features/area) drops dramatically for concentrations above 1.5 nM (see Figure S8). Therefore, it is clear that, in the absence of pH-induced disassembly, we indeed do see Au_{25} NC aggregation (while the STEM scans for pH-induced disassembly demonstrate the isolation of Au_{25} NCs into single NCs).

2.4. TPEF NSOM Experiments on Isolated Au_{25} Nanoclusters. As depicted in Figure 4, we used a femtosecond pulsed laser with 810 nm excitation wavelength coupled to a single-mode optical fiber for TPEF NSOM. The aperture diameter of the probe used for the current NSOM study was ~40 nm (see Supporting Information for SEM). Average near-field excitation powers used were ~600 μW. The highest TPEF NSOM counts observed were on the order of 30 000 cps. TPEF NSOM scans were conducted with 10 nm pixel sizes and

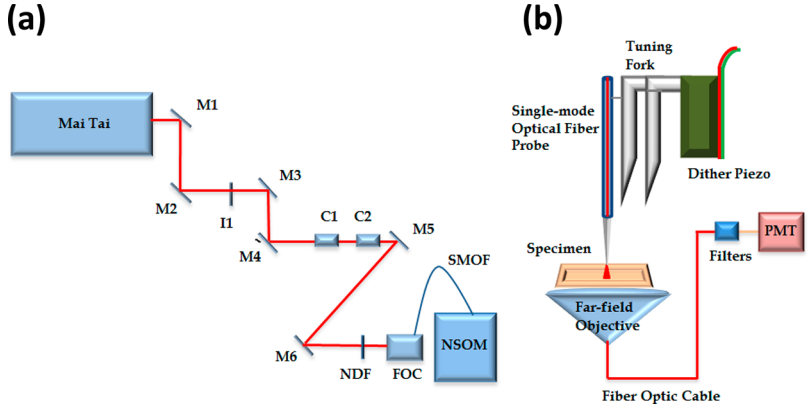

Figure 4. TPEF NSOM of Au_{25} single nanoclusters and the experimental setup. (a) The 810 nm femtosecond output from the Mai Tai laser source is coupled to a single-mode optical fiber. M1−M6, reflective mirrors; I1, iris; C1 and C2, collimating lenses; NDF, neutral density filter; FOC, fiber-optic coupler; SMOF, single-mode optical fiber. (b) Near-field illumination geometry inside the NSOM (tip−sample distance ≪ λ).

DOI: 10.1021/jacs.6b07737
J. Am. Chem. Soc. 2016, 138, 16299−16307

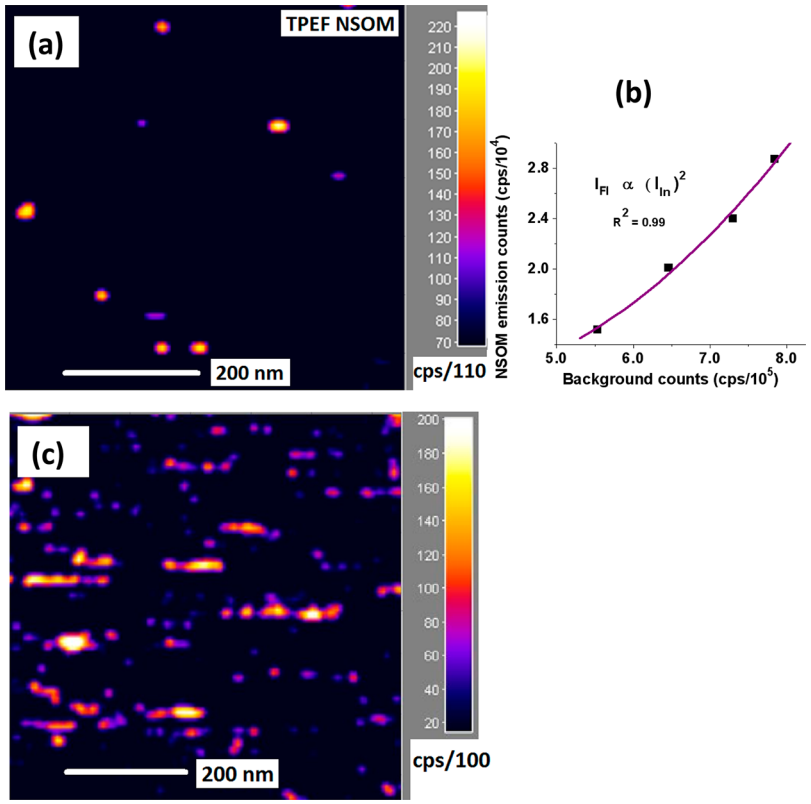

Figure 5. TPEF NSOM of Au_{25} single nanoclusters for samples prepared using 1.4 and 12.0 nM solutions. (a) TPEF NSOM image of $Au_{25}SG_{18}$ single NCs prepared by spin-coating 1.4 nM solution on plasma-cleaned glass. TPEF NSOM feature density is ~23 features/μm^2. TPEF counts observed for the highest intensity feature was ~25 000 cps for ~625 μW near-field excitation. (b) Plot of fluorescence intensity versus incident background intensity. The quadratic dependence proves TPEF response from the NSOM fluorescence. (c) TPEF NSOM image for a sample prepared by spin-coating 12.0 nM Au_{25} solution.

36 ms bin times. From the intensity-dependent TPEF NSOM scans, we confirmed the quadratic dependence of NSOM fluorescence intensity on incident background counts (Figure 5b): A corresponding slope for the log–log plot was ~1.77, which is nearly quadratic. (The TPEF NSOM response was reproduced for three different $Au_{25}SG_{18}$ NCs samples using the same sample preparation procedure.) The TPEF NSOM feature density was ~23 NCs/μm^2, which agrees well with the estimated isolated single NC densities (39 NCs/μm^2) derived from STEM/TEM data shown earlier. From the calculations in section 2.3, it can be concluded that the samples used for TPEF NSOM investigations indicated in Figure 5 had isolated single Au_{25} NCs on plasma-cleaned glass substrates separated by ~160 nm distances, which is much larger than the NSOM tip diameter of ~40 nm. This indicates that, with our sample preparation conditions, we can be confident that, on average, near-field two-photon excitation was localized on single isolated NCs. To our knowledge, this is the first report of isolated single NC TPEF NSOM. Additionally, our report of Au_{25} single NC investigations serves as the first report of *any* room-temperature monolayer-protected *stable* single NCs smaller than Au_{55} investigated in detail using *any* technique.[19] As mentioned earlier, Ag NCs show relatively low chemical stability, while Cu NCs are not reported to show significantly high TPA cross sections. Therefore, it is clear, according to our current work, that monolayer-protected Au_{25} NCs demonstrate their high optical stability and unusual optical properties when they are isolated from the ensemble. This puts protected Au_{25} NCs in a unique position, having unusual material and optical properties that are not collectively present in other noble metal NCs (i.e., in Ag NCs and Au NCs).

Also, the approach of isolating single NCs right at the beginning of dissolution allows one to avoid relying too much on other single molecule confirmatory techniques, such as fluorescence blinking, which could occur from more than a single NC due to inter-chromophore energy-transfer processes.[47] Additionally, as can be observed in Figure 5a, certain TPEF NSOM features are separated by <50 nm distances (as expected for a population of inter-nanocluster distances). This confirms that our TPEF NSOM excitation was able to excite individual NCs even when they were separated by distances of several tens of nanometers.

In order to understand the effect of concentration on TPEF NSOM feature density, we can compare the current data with the TPEF NSOM data obtained for a single NC sample (Figure 5c) prepared using 12.0 nM $Au_{25}(PET)_{18}$ solutions (PET = SCH_2CH_2Ph). The solution was sonicated for 1.5 min prior to spin-coating using the same conditions as before. As depicted in Figure 5c, most of the TPEF NSOM features observed seem to be larger (in the x–y plane) than the NSOM tip diameter (~40 nm). This is due to the individual NCs being in close proximity to one another on the substrate due to inter-nanocluster spacing that is smaller than the NSOM tip diameter and having many such single NCs in one field of view (hence elongated TPEF NSOM features). Using the STEM data depicted above, we calculated the expected NC density of the 12.0 nM sample to be ~334 NCs/μm^2 and the average inter-nanocluster distance to be ~55 nm. This indicates that, in the field of

DOI: 10.1021/jacs.6b07737
J. Am. Chem. Soc. 2016, 138, 16299–16307

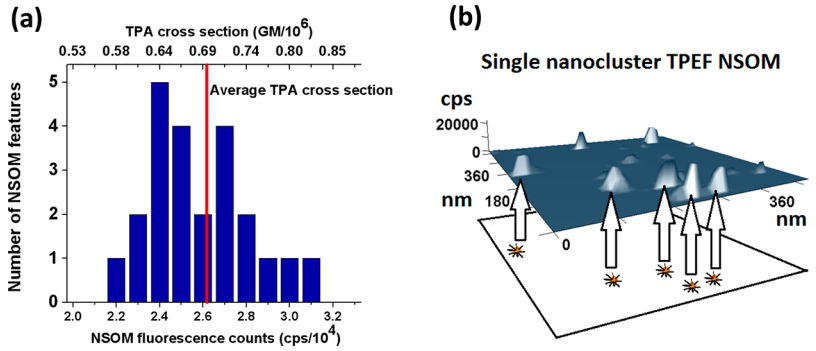

Figure 6. TPA cross section enhanced for Au_{25} single nanoclusters on plasma-cleaned glass substrate. (a) Histogram for 23 TPEF NSOM features and corresponding TPA cross sections. The average TPA cross section is enhanced on the solid phase compared to the solution phase counterpart. (b) Three-dimensional presentation of a TPEF NSOM image for quantum-confined single $Au_{25}SG_{18}$ NCs.

view of concern, some of the NCs could have inter-nanocluster distances that are smaller than the NSOM tip diameter, causing the TPEF NSOM features to overlap and form larger or elongated features (as can be predicted from Figure 5a, where inter-nanocluster distances <50 nm were observed when the *average* inter-nanocluster distance was ~160 nm). Therefore, our experimental evidence is consistent with the picture that, for 1.4 nM samples depicted in Figure 5a, the TPEF NSOM features observed indeed originated from isolated single NCs excited individually by TPEF NSOM.

2.5. Enhanced Two-Photon Absorption (TPA) Cross Section. Since it is clear that we have isolated single Au_{25} NCs by TPEF NSOM, the TPA cross section can be estimated for single Au_{25} NCs from the NSOM fluorescence intensity observed. As can be seen in Figure 6a, the TPA cross section histogram for the 23 features indicated a somewhat non-Gaussian distribution. The average TPA cross section calculated (δ_{solid} = 6.99 × 10^5 GM) appears to be enhanced by ~64% compared to the solution-phase counterpart. This completely unexpected enhancement in TPA cross section deserves further investigation.

Since the TPA cross section is a third-order nonlinear optical property (imaginary part of χ^3), the enhanced δ_{solid} value observed can be attributed to a local field enhancement due to changes in the refractive indices. On solid glass coverslips, it can be assumed that Au_{25} NCs are surrounded mainly by air ($n \approx 1.00$). The solvent dielectric environment reported by Ramakrishna et al.[15] (for hexane, n = 1.375) has a higher refractive index. It can be inferred that a local field enhancement in χ^3 caused an enhanced δ_{solid} value. Interestingly, a similar enhancement of χ^3 (real component) was reported by Wang et al.[48] for nanometer-sized CdS clusters.

To interpret the enhancement observed, the TPA process with respect to a two-level approximation can be considered.[49] It is clear that there is an enhancement in the difference between the dipole moments of the excited-state with respect to the ground-state $\Delta\mu_{10}$ (~33%) when the NCs were placed on the solid substrate (see Supporting Information). This additional enhancement (that cannot be explained by changes in the refractive indices) can be attributed to a local field-induced dipole moment change due to a change in polarizability of the excited state with respect to the ground state.[50,51] A similar enhancement of $\Delta\mu_{10}$ in the electric-field-sensitive protein mCherry was previously reported by Rebane and co-workers.[52] This implies that local field effects on single Au_{25} NCs are enhancing the TPA cross sections, improving their sensitivity to the environment.

In order to further understand this effect, we have utilized models related to the few-atom local field enhancement predicted for "magic" number systems[53] and local field-induced microscopic cascading effects[54−57] on the third-order nonlinear response. Interestingly, from our calculations, we obtain enhancement factors ranging from 1.5 to 10 for Au_{25} NC systems! From previous theoretical and experimental work by Bloembergen and co-workers[54] and Boyd and co-workers,[55,56] it has been demonstrated that the local field effects can create cascaded contributions of the second-order polarization to the third-order susceptibility. Interestingly, Kaplan and Volkov have theoretically predicted that nanoscale (near-field) local field enhancement effects may be possible for certain "magic" numbered 1D or 2D systems such as quantum clusters.[53] We think our observation of an enhanced TPA cross section for Au_{25} NCs serves as the *first such experimental evidence* of a material that shows few-atom local field enhancement induced nonlinear cascading predicted for quantum cluster systems. Further investigations on Au_{25} NC nonlinear optical properties may reveal a more detailed picture of this effect. Therefore, as indicated by Boyd[56] and Volkov,[53] our results suggest that Au_{25} NCs can potentially be used as chromophores in ultrasensitive biosensing, molecular computers, and molecular logic.

2.6. Superior Point Resolution for Aperture-Based TPEF NSOM. As shown in Figure 7, the lateral point resolution is significantly better than the typical resolution for confocal fluorescence microscopy (~200 nm)[58] and previously reported TPEF NSOM resolution of 175 nm for Rhodamine B single molecules.[35] For the TPEF NSOM feature with S/N ≈ 7, the point resolution observed was ~30 nm (~λ/27), which is a 5-fold improvement in point resolution for the same technique (see Supporting Information for the Gaussian fitting of data without smoothening). Moreover, it could be argued that the TPEF NSOM point resolution observed is better than the probe diameter (~40 nm), which can be attributed to the intensity dependence of TPEF NSOM that reduces the size of the excitation PSF compared to its one-photon counterpart. Therefore, with the point resolution around several tens of nanometers obtained from the current approach, we were able to excite and interrogate isolated NCs one at a time (on the solid substrate). Also, the fact that we were able to observe a point resolution (30 nm) 5-fold better than the previous resolution (~175 nm) for the same aperture-based TPEF NSOM technique can be attributed to the unusually large TPA

DOI: 10.1021/jacs.6b07737
J. Am. Chem. Soc. 2016, 138, 16299−16307

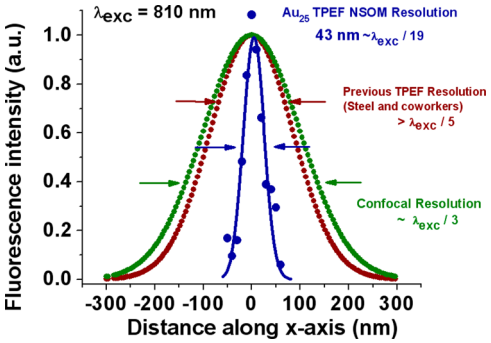

Figure 7. TPEF NSOM point resolution reaches 30 nm with Au_{25} clusters. Comparison between transverse point resolution attainable with confocal fluorescence microscopy, previous aperture-based TPEF NSOM, and the current approach. The point resolution 43 ± 7 nm (~λ/19) fwhm for TPEF NSOM of $Au_{25}SG_{18}$ single nanoclusters (blue) in the current work (from a feature with S/N ≈ 7) evidently surpasses the previously observed value. Also, the point resolution without averaging adjacent points (without smoothening) produces 30 ± 5 nm (~λ/27) resolution for the same image, which is greater than 5-fold improvement for the aperture-based TPEF NSOM technique.

cross section of these isolated single NCs and their high photostability compared to many organic chromophores.

3. CONCLUSION

It is clear that an enhanced two-photon absorption cross section of 25-atom gold nanoclusters due to local field effects and their high photostability under two-photon near-field excitation was revealed while interrogating them using aperture-based TPEF NSOM. We attribute the unusually enhanced TPA cross section of isolated single NCs to few-atom local field enhancement predicted for "magic" number systems that may possess enhancement factors up to 10 for Au_{25}! The superior resolution observed was otherwise not possible with typical organic chromophores. Therefore, we can state that we have employed (and unveiled) the unique properties of these quantum-confined NC materials while optically detecting and investigating them (and *any* NC) for the first time at single NC concentrations.

In summary, by taking advantage of the unique optical properties of an emergent nanomaterial (Au NCs) and using high-resolution nonlinear near-field microscopy (TPEF NSOM), we have optically interrogated single isolated Au NCs of ~1.2 nm diameter. To our knowledge, the point resolution reported (~30 nm) in this study is the best observed for the aperture-based TPEF NSOM imaging (5-fold improvement) that has rendered two-photon excitation of individual NCs that are separated by <50 nm distances. Furthermore, as confirmed in this work, the ability to obtain isolated NCs in solution and on solid substrate introduces a method to unambiguously control and confirm the single molecule nature of the experiment, which can also be utilized in studies with many similar glutathione-capped single NP/NCs. The observed enhancement (64%) in the average TPA cross section (when the NCs were moved from solution ensemble to isolated single NCs) can be attributed to the few-atom local field enhancement effects. Also, the heterogeneity and the asymmetry of the observed distribution in the two-photon cross section indicates possible heterogeneous distribution of local field strengths.

The current approach of employing the unusually large TPA cross sections and photostability of single Au_{25} NCs in TPEF NSOM can be used for future single NC investigations. Additionally, TPEF of these NCs can potentially be used in ultrasensitive sensing of local fields to probe their local nanoenvironments. Therefore, this study indicates that single Au_{25} NCs may be used in sensing of biological systems (e.g., proteins) that can make nanoenvironments with varying local fields. For example, in Alzheimer's disease, the formation of certain amyloid beta aggregates is induced by the presence of increased metal ion concentrations.[59−62] Since local accumulation of metal ions can cause enhanced local electric fields, TPEF imaging using Au_{25} NCs can be a promising approach to diagnose early onset of diseases such as Alzheimer's. Therefore, Au_{25} NCs, with their local field-sensitive two-photon response (and the use of more biologically transparent two-photon excitation wavelengths), are promising candidates for imaging and diagnostics of biological tissues. Our recent studies clearly suggest that the Au_{25} NCs can be inserted into biological cells without any apparent toxicity and can be used subsequently in cellular imaging applications.[62] Also, we were able to observe accelerated damage of cells when cell-inserted Au_{25} NCs were excited using laser irradiation, indicating the potential to use them in cancer cell therapy.

4. EXPERIMENTAL SECTION

4.1. Synthesis of $Au_{25}SG_{18}$. The Au_{25} capped with glutathione (SG) was synthesized in two steps as follows.

4.1.1. Synthesis of Au_nSG_m Clusters. A 0.1698 g portion of $HAuCl_4$ was dissolved in 100 mL of methanol and stirred at 0 °C (ice bath) for 15 min. Following the dissolution (and cooling) step, 0.614 g of glutathione (GSH) was added to the mixture, and the reaction was left to proceed (while stirring) for another 30 min. Subsequently, 0.1891 g of $NaBH_4$ was dissolved in 25 mL of water and added dropwise into the reaction mixture. The reaction was further run for another 1 h. All of the aforementioned steps were conducted in a 0 °C ice bath. After the reaction with $NaBH_4$ was complete (i.e., after 1 h), the resulting reaction mixture was centrifuged, and the precipitate was washed three times with methanol (vortex, sonicate, and then centrifuge), followed by drying in a vacuum at room temperature.

4.1.2. Etching of Au_nSG_m Clusters To Obtain Monodisperse $Au_{25}SG_{18}$ Nanoclusters. The resulting Au_nSG_m clusters (82 mg) were dissolved in 7 mL of water and heated in a water bath at 55 °C, followed by the addition of a 132 mg portion of GSH. (Water bath was set up at least an hour prior to the beginning of the experiment, and the temperature was set at 55 °C, which was maintained throughout the experiment). The reaction was stirred slowly (~300−400 rpm; not faster than that) for 4 h. The reaction mixture was then centrifuged, followed by discarding of the precipitate. The resulting supernatant was transferred to a new centrifuge tube, followed by the addition of 2−3 mL of ethanol to precipitate $Au_{25}SG_{18}$ NCs. This precipitate was further purified three times by dissolution (by water) and precipitation (by ethanol) cycles to obtain monodisperse $Au_{25}SG_{18}$ NCs. The solid NC sample was then dried in a vacuum at room temperature and subsequently stored in the freezer. We used Millipore-grade water for all of our synthesis and purification steps. Also, all of the solvents used were of spectroscopic grade (or better). All of our glassware was cleaned in a base bath for 24 h, followed by rinsing with Millipore water and oven-drying for 12 h before being used.

4.2. Sample Preparation for TPEF NSOM. $Au_{25}SG_{18}$ NCs were dissolved in pH = 7.2 water and filtered using 220 nm pore PTFE filters to remove undissolved large aggregates. The solutions were sonicated for 1 min to dissolve any aggregated clusters and then diluted (in a series of dilutions) to obtain 1.4 nM concentrations of $Au_{25}SG_{18}$ NCs. Subsequently, following another 1 min sonication time and a filtering step (using 220 nm pore PTFE filters), a 4 μL volume of the solution (using a calibrated micropipet) was spin-coated on a plasma-cleaned glass substrate at 1400 rpm for 40 s. The resulting glass substrates were vacuum-dried under ~10 in. Hg at 40 °C for 2.5 h.

DOI: 10.1021/jacs.6b07737
J. Am. Chem. Soc. 2016, 138, 16299−16307

The dried and cooled (to room temperature under vacuum) samples were then used for TPEF NSOM imaging and spectroscopy.

4.3. TPEF NSOM Experiment. A Mai Tai femtosecond laser source with a repetition rate of 80 MHz was used for the excitation (see Figure 3). Pulses of ~110 fs (fwhm) at 810 nm were coupled to a single-mode optical fiber (maximum throughput at ~780 nm), and the tapered end of the optical fiber served as the local excitation source for the NSOM setup (Mo Scan NSOM setup by CDP systems, see ref 63 for previous work with this setup). Near-field illumination of the sample generates the TPEF from single Au NCs. Raster scanning of the 1 μm × 1 μm areas with 10 nm pixels at 36 ms bin times generated TPEF NSOM images. Fluorescence emission of the single Au NCs and transmitted 810 nm photons was collected using a far-field inverted objective and transferred through a fiber-optic cable to a photomultiplier tube. As shown in Figure 3d, the transmitted 810 nm light is sent through a filter housing and attenuated using two 808 nm notch filters and a short-pass filter. Thus, the anti-Stokes-shifted TPEF can be detected (in the visible region) with sufficient intensities for single molecule imaging. The TPEF NSOM intensities were analyzed using FemtoScan Online software, and Gaussian fits for the TPEF NSOM point resolution were obtained using Origin 7 fitting software. The final TPEF NSOM scans were displayed using ImageJ software.

4.4. STEM Characterization. $Au_{25}SG_{18}$ NCs were dissolved in pH = 7.2 water and filtered using 220 nm pore PTFE filters to remove undissolved large aggregates. The solutions were sonicated for 1 min to dissolve any aggregated clusters and then diluted to obtain 120 nM concentrations of $Au_{25}SG_{18}$ NCs. Following another filtering step (using 220 nm pore PTFE filters), a 1 μL volume of the solution (using a calibrated micropipet) was drop-cast on a 200-mesh holey-carbon copper grid and dried in air for >10 min. The copper grids were purchased from SPI Supplies and were used as received. Subsequently, the samples were characterized using STEM with a JEM-2100F electron microscope with a CEOS probe corrector. The size distribution histograms were analyzed using ImageJ software.

■ ASSOCIATED CONTENT

Supporting Information

The Supporting Information is available free of charge on the ACS Publications website at DOI: 10.1021/jacs.6b07737.

Additional TPEF NSOM data, TEM analysis, detailed calculations described in the article, SEM of NSOM probe tip, Gaussian fitting for point resolution, pH-dependent absorption spectrum, and NC aggregation in the absence pH-induced disassembly, including Figures S1−S8 (PDF)

■ AUTHOR INFORMATION

Corresponding Author

*tgoodson@umich.edu

Notes

The authors declare no competing financial interest.

■ ACKNOWLEDGMENTS

N.A. gratefully acknowledges Dr. Oleg Varnavski, Dr. Jeffery E. Raymond, Dr. Sung-Hei Yau, and Rosina Ho Wu for helpful discussions. T.G. would like to acknowledge U.S. Army Research Office Materials Research Directorate under Grant No. W911 NF-13-1-0314 and NSF Grant No. 1306815 for support of this research. The JEOL JEM-2100F microscope was supported by NSF Grant No. DMR-0723032.

■ REFERENCES

(1) Jadzinsky, P. D.; Calero, G.; Ackerson, C. J.; Bushnell, D. A.; Kornberg, R. D. *Science* **2007**, *318*, 430.

(2) Li, Z. Y.; Young, N. P.; Di Vece, M.; Palomba, S.; Palmer, R. E.; Bleloch, A. L.; Curley, B. C.; Johnston, R. L.; Jiang, J.; Yuan, J. *Nature* **2008**, *451*, 46.

(3) Zhu, M.; Aikens, C. M.; Hollander, F. J.; Schatz, G. C.; Jin, R. *J. Am. Chem. Soc.* **2008**, *130*, 5883.

(4) Heaven, M. W.; Dass, A.; White, P. S.; Holt, K. M.; Murray, R. W. *J. Am. Chem. Soc.* **2008**, *130*, 3754.

(5) Desireddy, A.; Conn, B. E.; Guo, J.; Yoon, B.; Barnett, R. N.; Monahan, B. N.; Kirschbaum, K.; Griffith, W. P.; Whetten, R. L.; Landman, U.; Bigioni, T. P. *Nature* **2013**, *501*, 399.

(6) Yang, H.; Wang, Y.; Huang, H.; Gell, L.; Lehtovaara, L.; Malola, S.; Hakkinen, H.; Zheng, N. *Nat. Commun.* **2013**, *4*, 2422.

(7) Azubel, M.; Koivisto, J.; Malola, S.; Bushnell, D.; Hura, G. L.; Koh, A. L.; Tsunoyama, H.; Tsukuda, T.; Pettersson, M.; Hakkinen, H.; Kornberg, R. D. *Science* **2014**, *345*, 909.

(8) Lopez-Acevedo, O.; Kacprzak, K. A.; Akola, J.; Hakkinen, H. *Nat. Chem.* **2010**, *2*, 329.

(9) Chen, S.; Ingram, R. S.; Hostetler, M. J.; Pietron, J. J.; Murray, R. W.; Schaaf, T. G.; Khoury, J. T.; Alvarez, M. M.; Whetten, R. L. *Science* **1998**, *280*, 2098.

(10) Zhu, M.; Aikens, C. M.; Hendrich, M. P.; Gupta, R.; Qian, H.; Schatz, G.; Jin, R. *J. Am. Chem. Soc.* **2009**, *131*, 2490.

(11) Yau, S. H.; Varnavski, O.; Goodson, T., III. *Acc. Chem. Res.* **2013**, *46*, 1506.

(12) Varnavski, O.; Ramakrishna, G.; Kim, J.; Lee, D.; Goodson, T. *J. Am. Chem. Soc.* **2010**, *132*, 16.

(13) Yuan, X.; Setyawati, M. I.; Tan, A. S.; Ong, C. N.; Leong, D. T.; Xie, J. *NPG Asia Mater.* **2013**, *5*, e39.

(14) Yau, S. H.; Abeyasinghe, N.; Orr, M.; Upton, L.; Varnavski, O.; Werner, J. W.; Yeh, H.-C.; Sharma, J.; Shreve, A. P.; Martinez, J. S.; Goodson, T., III. *Nanoscale* **2012**, *4*, 4247.

(15) Ramakrishna, G.; Varnavski, O.; Kim, J.; Lee, D.; Goodson, T. *J. Am. Chem. Soc.* **2008**, *130*, 5032.

(16) Moerner, W. E.; Fromm, D. P. *Rev. Sci. Instrum.* **2003**, *74*, 3597.

(17) Scholl, J. A.; Koh, A. L.; Dionne, J. A. *Nature* **2012**, *483*, 421.

(18) Bahena, D.; Bhattarai, N.; Santiago, U.; Tlahuice, A.; Ponce, A.; Bach, S. B. H.; Yoon, B.; Whetten, R. L.; Landman, U.; Jose-Yacaman, J. *J. Phys. Chem. Lett.* **2013**, *4*, 975.

(19) Jian, N.; Stapelfeldt, C.; Hu, K.-J.; Froba, M.; Palmer, R. E. *Nanoscale* **2015**, *7*, 885.

(20) Rittweger, E.; Han, K. Y.; Irvine, S. E.; Eggeling, C.; Hell, S. W. *Nat. Photonics* **2009**, *3*, 144.

(21) Hell, S. W. *Nat. Biotechnol.* **2003**, *21*, 1347.

(22) Hell, S. W. *Science* **2007**, *316*, 1153.

(23) Westphal, V.; Kastrup, L.; Hell, S. W. *Appl. Phys. B: Lasers Opt.* **2003**, *77*, 377.

(24) Betzig, E.; Chichester, R. J. *Science* **1993**, *262*, 1422.

(25) Betzig, E.; Trautman, J. K. *Science* **1992**, *257*, 189.

(26) Xie, X. S.; Dunn, R. C. *Science* **1994**, *265*, 361.

(27) Trautman, J. K.; Macklin, J. J.; Brus, L. E.; Betzig, E. *Nature* **1994**, *369*, 40.

(28) Betzig, E.; Trautman, J. K.; Harris, T. D.; Weiner, J. S.; Kostelak, R. L. *Science* **1991**, *251*, 1468.

(29) Betzig, E.; Lewis, A.; Harootunian, A.; Isaacson, M.; Kratschmer, E. *Biophys. J.* **1986**, *49*, 269.

(30) Sanchez, E. J.; Novotny, L.; Xie, X. S. *Phys. Rev. Lett.* **1999**, *82*, 4014.

(31) Grotjohann, T.; Testa, I.; Leutenegger, M.; Bock, H.; Urban, N. T.; Lavoie-Cardinal, F.; Willig, K. I.; et al. *Nature* **2011**, *478*, 204.

(32) Denk, W.; Strickler, J. H.; Webb, W. W. *Science* **1990**, *248*, 73.

(33) Jarrett, J. W.; Zhao, T.; Johnson, J. S.; Knappenberger, K. L., Jr. *J. Phys. Chem. C* **2015**, *119*, 15779.

(34) Jarrett, J. W.; Zhao, T.; Johnson, J. S.; Liu, X.; Nealey, P. F.; Vaia, R. A.; Knappenberger, K. L., Jr. *J. Phys. Chem. Lett.* **2016**, *7*, 765.

(35) Lewis, M. K.; Wolanin, P.; Gafni, A.; Steel, D. G. *Opt. Lett.* **1998**, *23*, 1111.

(36) Ho-Wu, R.; Yau, S. H.; Goodson, T., III. *ACS Nano* **2016**, *10*, 562.

(37) Wu, Z.; Jin, R. *Nano Lett.* **2010**, *10*, 2568.

DOI: 10.1021/jacs.6b07737
J. Am. Chem. Soc. 2016, 138, 16299−16307

(38) Dulkeith, E.; Niedereichholz, T.; Klar, T. A.; Feldmann, J.; von Plessen, G.; Gittins, D. I.; Mayya, K. S.; Caruso, F. *Phys. Rev. B: Condens. Matter Mater. Phys.* **2004**, *70*, 205424.
(39) Goodson, T., III; Varnavski, O.; Wang, Y. *Int. Rev. Phys. Chem.* **2004**, *23*, 109.
(40) Mooradian, A. *Phys. Rev. Lett.* **1969**, *22*, 185.
(41) Wu, Z.; Suhan, J.; Jin, R. *J. Mater. Chem.* **2009**, *19*, 622.
(42) Qian, H.; Zhu, M.; Wu, Z.; Jin, R. *Acc. Chem. Res.* **2012**, *45*, 1470.
(43) Zhu, M.; Lanni, E.; Garg, N.; Bier, M. E.; Jin, R. *J. Am. Chem. Soc.* **2008**, *130*, 1138.
(44) Negishi, Y.; Chaki, N. K.; Shichibu, Y.; Whetten, R. L.; Tsukuda, T. *J. Am. Chem. Soc.* **2007**, *129*, 11322.
(45) Kirchner, C.; Liedl, T.; Kudera, S.; Pellegrino, T.; Munoz-Javier, A.; Gaub, H. E.; Stolzle, S.; Fertig, N.; Parak, W. J. *Nano Lett.* **2005**, *5*, 331.
(46) Negishi, Y.; Nobusada, K.; Tsukuda, T. *J. Am. Chem. Soc.* **2005**, *127*, 5261.
(47) Yip, W.-T.; Hu, D.; Yu, J.; Vanden Bout, D. A.; Barbara, P. F. *J. Phys. Chem. A* **1998**, *102*, 7564.
(48) Wang, Y.; Herron, N. *J. Phys. Chem.* **1991**, *95*, 525.
(49) Drobizhev, M.; Makarov, N. S.; Hughes, T.; Rebane, A. *J. Phys. Chem. B* **2007**, *111*, 14051.
(50) Drobizhev, M.; Makarov, N. S.; Tillo, S. E.; Hughes, T.; Rebane, A. *Nat. Methods* **2011**, *8*, 393.
(51) Ponder, M.; Mathies, R. *J. Phys. Chem.* **1983**, *87*, 5090.
(52) Drobizhev, M.; Scott, J. N.; Callis, P. R.; Rebane, A. *IEEE Photonics J.* **2012**, *4*, 1996.
(53) Kaplan, A. E.; Volkov, S. N. *Phys. Rev. Lett.* **2008**, *101*, 133902.
(54) Bedeaux, D.; Bloembergen, N. *Physica* **1973**, *69*, 57.
(55) Dolgaleva, K.; Boyd, R. W.; Sipe, J. E. *Phys. Rev. A: At., Mol., Opt. Phys.* **2007**, *76*, 063806.
(56) Baev, A.; Autschbach, J.; Boyd, R. W.; Prasad, P. N. *Opt. Express* **2010**, *18*, 8713.
(57) Dolgaleva, K.; Boyd, R. W. *Adv. Opt. Photonics* **2012**, *4*, 1.
(58) Cox, G.; Sheppard, C. J. R. *Microsc. Res. Tech.* **2004**, *63*, 18.
(59) Huang, X.; Atwood, C. S.; Moir, R. D.; Hartshorn, M. A.; Vonsattel, J.-P.; Tanzi, R. E.; Bush, A. I. *J. Biol. Chem.* **1997**, *272*, 26464.
(60) Atwood, C. S.; Moir, R. D.; Huang, X.; Scarpa, R. C.; Bacarra, N. M.; Romano, D. M.; Hartshorn, M. A. J.-P.; Tanzi, R. E.; Bush, A. I. *J. Biol. Chem.* **1998**, *273*, 12817.
(61) Curtain, C. C.; Ali, F.; Volitakis, I.; Cherny, R. A.; Norton, R. S.; Beyreuther, K.; Barrow, C. J.; Masters, C. L.; Bush, A. I.; Barnham, K. J. *J. Biol. Chem.* **2001**, *276*, 20466.
(62) Using live cells, we have conducted cell-insertion studies of water-soluble Au_{25} NCs. We excited the cells using increasing laser intensities, which indicated a clear signature of cell insertion in live cells and retention of the NCs while the imaging was conducted. Accelerated cell damage was observed for NC-inserted cells, indicating the potential to conduct cancer cell therapy. No cell toxicity of the NCs was observed throughout the study. This work will be submitted soon in a separate article.
(63) Raymond, J. E.; Goodson, T., III. *J. Phys. Chem. Lett.* **2011**, *2*, 329.

DOI: 10.1021/jacs.6b07737
J. Am. Chem. Soc. 2016, 138, 16299−16307